Downconversion efficiency in backward optical parametric oscillators

Carlos Montes, Marc de Micheli, Pierre Aschieri

Downconversion efficiency in backward optical parametric oscillators

Carlos Montes, Marc de Micheli, and Pierre Aschieri

Laboratoire de Physique de la Matière Condensée (CNRS UMR 7336),
Université de Nice-Sophia Antipolis, Parc Valrose, F-06108 Nice Cedex2, France
Correspondence author: Email: carlos.montes@unice.fr

Abstract

In optical parametric oscillators based on periodically poled (PP) nonlinear quadratic materials, choosing a submicronic poling period allows generating the phase-matched signal and idler waves in opposite directions. In this case a distributed feedback mechanism is established, which enables optical parametric oscillation without the need of external mirrors or surface coatings. A backward mirrorless optical parametric oscillator (BMOPO), has been experimentally realized using a periodically-poled $KTiOPO_4$ (PPKTP) crystal with sub-μm periodicity as a quasi-phase-matched (QPM) nonlinear medium. A remarkable property of the BMOPO is the strong asymmetry in spectral bandwidth between the signal and the idler pulses: the bandwidth of the co-propagating forward wave is comparable to the pump bandwidth, whereas that of the backward wave is typically one to two orders of magnitude narrower. It has been recently demonstrated both experimentally and numerically for a pump wave exhibiting deterministic phase modulation in the PPKTP BMOPO. This property is studied here in a guided wave configuration for broad incoherent pump pulses with bandwidth up to 4.7 THz. We demonstrate that in this case the higher the incoherence of the pump, the larger the amount of coherence transfer. The group velocities of the forward propagating waves can be perfectly matched by an appropriate waveguide profile in order to optimize the coherence transfer to the backward propagating wave. However, a nanometric QPM periodicity is required for perfect group velocity matching of the pump with the forward idler wave. Up to now such short periods have been only achieved by epitaxy in GaN. In order to have long enough waveguides we have studied this process in a PPGaN waveguide presenting stitching errors, which are very likely to occur during the fabrication process of the waveguide. We model a BMOPO in a fragmented GaN waveguide consisting of a sequence of submicronic PP elements separated by uniformly polarized connection sections representing the stitching errors. We have shown that in these fragmented waveguides the coherence transfer is nonintuitivelly almost as high as for a single piece PP waveguide because the generated coherent phase of the backscattered wave locks the phases of the forward propagating waves in such a way that the dynamics is almost insensitive to the short connection sections. We analyse on a large pump bandwidth range the downconversion efficiency versus the stochastic pump bandwidth for two different fragmented PPGaN BMOPOs and we compare it to the one piece periodically polarized PPGaN BMOPO.

Keywords: Coherence gain; Nonlinear optical waveguides; Parametric oscillators; Parametric downconversion; Semiconductor nonlinear optics;

1 Introduction

In optical nonlinear quadratic materials, the periodically poled (PP) technique allows to build optical parametric oscillators (cf. Fig. 1). It is possible to choose a submicronic poling period such that the phase-matched signal and idler waves are generated in opposite directions [1] correspondig to configurations of Fig. 1(b)(c). In these cases, a distributed feedback mechanism is established, which enables optical parametric oscillation without the need of external mirrors or surface coatings. The backward mirrorless optical parametric oscillator (BMOPO) has been experimentally realized in the configuration of Fig. 1(b) using a periodically-poled $KTiOPO_4$ (PPKTP) crystal with 800 nm periodicity as a quasi-phase-matched (QPM) nonlinear medium [2].

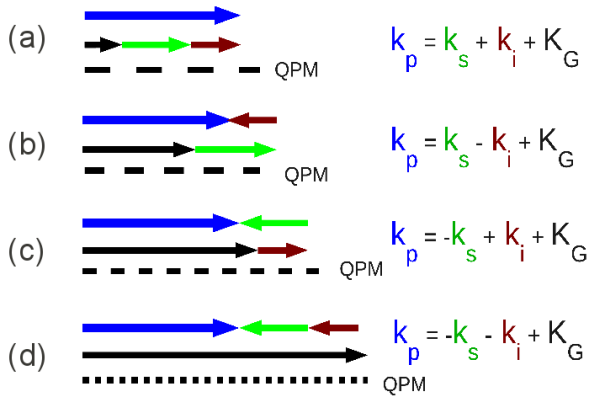

Figure 1: Wave vector diagrams (momentum conservation) for the non-degenerate three-wave interaction in an OPO : from top to bottom, (a) three wave forward configuration; (b) singly backward idler configuration; (c) singly backward signal configuration; and (d) doubly backward (signal and idler) configuration. As we can see the QPM grating show a decreasing phase-reversal period for the nonlinear susceptibilty represented by the bold broken lines under each configuration.

One of the remarkable properties of the BMOPO is the strong asymmetry in spectral bandwidth between the signal and the idler pulses: the bandwidth of the co-propagating forward wave is comparable to the pump bandwidth, whereas that of the backward wave is typically one to two orders of magnitude narrower. This has been recently demonstrated both experimentally and numerically for a pump wave exhibiting deterministic phase modulation in the PPKTP BMOPO for relatively narrowband (1.2 THz) linearly-chirped pump pulses [3] and relatively broadband (4 THz) pump pulses too [4]. In accordance with the convection-induced phase-locking mechanism [5, 6, 7, 8, 9], the phase modulation in the pump is coherently transferred to the forward parametric wave, while the backward wave retains a narrow bandwidth and high coherence. This property is studied here for broad incoherent pump pulses up to 4.7 THz. We demonstrate that in this case the higher the incoherence of the pump, the larger the amount of coherence transfer. The group velocities of the forward propagating waves can be perfectly matched by an approriate waveguide profile in order to optimize the coherence transfer to

the backward propagating wave, corresponding to the configuration of Fig. 1(c). However, a nanometric QPM periodicity is required for perfect group velocity matching of the pump and the forward propagating idler wave. Up to now, this can be only achieved by epitaxy in a GaN material. Asymmetric GaN waveguides grown on (0001) sapphire by molecular beam epitaxy or by metal-organic chemical vapor deposition are promising structures for applications in nonlinear optics. Periodically poled GaN (PPGaN) was used for second harmonic generation [10] and the possibility to grow submicronic PP GaN films [11] opens the door for parametric counterpropagating oscillation thanks to reasonably large second order susceptibility ($\chi_{33}^{(2)} = 10.6$ pm/V measured in [12]), comparable to KTP. We have studied this process in a PPGaN waveguide presenting stitching errors, which are very likely to occur during the fabrication process of the waveguide. Indeed, the realization of centimeter long devices presenting a submicrometer periodicity is not possible without moving the sample under the writing beam. This displacement introduces the stitching faults. The device is then formed by a sequence of PP poled elements of about 200 μm long (PPGaN bricks) separated by uniformly polarized connection sections of several micrometers long representing the stitching errors. We have shown that the coherence transfer is nonintuitivelly almost as high as for a single piece periodically polarized waveguide [13], because the generated coherent phase of the backscattered wave locks the phases of the forward propagating waves in such a way that the dynamics is almost insensitive to the short connection sections. Here we analyse the downconversion efficiency versus the stochastic pump bandwidth for two different fragmented PPGaN BMOPOs in a large frequency pump bandwidth range and compare it to the one piece periodically polarized PPGaN BMOPO. The BMOPO dynamics is numerically simulated with a new numerical scheme that solves the coupled wave equations in the counterpropagating configuration in the presence of group-velocity dispersion (GVD) by combining the trajectory method for the nonlinear three-wave interaction, extensively used for the treatment of stimulated Brillouin backscattering problems [14, 15], with fast Fourier transformation (FFT) to account for the group-velocity dispersion effects in the spectral domain [16, 4].

2 BMOPO model in a fragmented waveguide

In a BMOPO, the pump wave is down-converted into forward-propagating and backward-propagating parametric waves, in accordance with energy conservation, $\omega_p = \omega_f + \omega_b$ and counterpropagating quasi-phase matching, $k_p - k_f + k_b = K_G$, where $j = p, f, b$ denote the pump, the forward and the backward parametric waves, respectively. $K_G = 2\pi/\Lambda_G$ is the grating vector given by Λ_G, the modulation period of the second-order nonlinear coefficient. The coherence transfer effect to the backward wave is especially pronounced when the pump wavelength and the modulation period of the nonlinear medium are chosen so that the group velocities of the pump and the forward wave are exactly matched [6]. This configuration may be achieved in a GaN waveguide with a group velocity dispersion modified by a particular profile of the refractive index, a technique widely used in fiber to compensate the material dispersion with the waveguide dispersion [17]. Then it is able to exactly match the pump and the idler group velocities and the counterpropagating wave will be the signal, corresponding to Fig. 1(c). However,

this requires a short PP period Λ_G of hundreds of nm in length, which may be realized in the GaN structure thanks to epitaxy [11, 12]. For z-polarized waves in PPGaN, matching group velocities can be achieved by designing the experiment so that the pump and the forward wave are on different sides of the maximum on the group-velocity curve shown in Fig. 2. This shape of group-velocity curve may be obtained in the guided PPGaN structure composed of a strip-loaded GaN waveguide of 2 μm width and 1.8 μm depth on a AlInN buffer which has been realized on sapphire substrate by epitaxy. The Sellmeier relation given in [12] is used for material dispersion, and finite waveguide dispersion corrections [17] yield the corresponding group-velocity curve of Fig. 2.

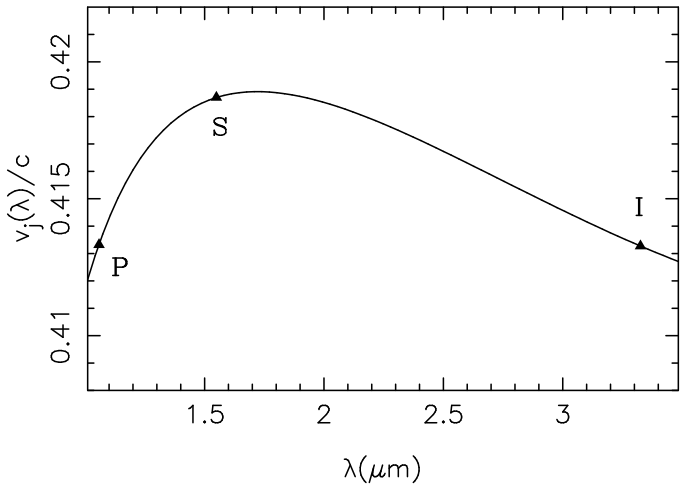

Figure 2: Group velocity for the z-polarized waves in GaN as function of the wavelength, calculated from the Sellmeier expansions in [12] with a particular profile of the refractive index of the guide [17]. The triangles mark the configuration of perfectely matched pump and idler group velocities ($|\mathrm{v_p} - \mathrm{v_i}| = 0$), and are labeled **P** for the pump, **S** for the signal, and **I** for the idler.

The pump intensity required to reach threshold for BMOPO operation, $I_{p,th}$, can be estimated from the plane-wave monochromatic model for the undepleted pump parametric approximation [1] as $I_{p,th} = c\varepsilon_0 n_p n_f n_b \lambda_f \lambda_b / 2L^2 d_{eff}^2$, where c is the speed of light in vacuum, ε_0 is the permittivity of free space, n_j denotes the refractive indices, λ_j denotes the backward and forward wavelengths, L is the nonlinear interaction length and $d_{eff} = 7$ pm/V is the effective quadratic nonlinearity.

Numerical simulations of the nonlinear three-wave interactions in a BMOPO solve the coupled wave equations in the slowly-varying-envelope approximation. The parameters used in the model are those of a periodically poled GaN waveguide (PPGaN) grown by epitaxy on sapphire substrates [10] and presenting submicronic periodicity of the $\chi^{(2)}$ coefficient [11], which measure in [12], yields $d_{eff} = (2/\pi)\chi_{33}^{(2)} = 7$ pm/V. The field amplitudes, $\mathbf{A_j}$ ($\mathbf{j} = \mathbf{p}, \mathbf{s}, \mathbf{i}$), of the pump and the parametric backward signal wave and forward idler wave, evolve with the

coupled equations:

$$\begin{aligned}
(\partial_t + \mathrm{v_p}\partial_x + \gamma_p + i\beta_p\partial_{tt})\,\mathbf{A_p} &= -\sigma_p(x)\mathbf{A_s}\mathbf{A_i} \\
(\partial_t - \mathrm{v_s}\partial_x + \gamma_s + i\beta_s\partial_{tt})\,\mathbf{A_s} &= \sigma_s(x)\mathbf{A_p}\mathbf{A_i^*} \\
(\partial_t + \mathrm{v_i}\partial_x + \gamma_i + i\beta_i\partial_{tt})\,\mathbf{A_i} &= \sigma_i(x)\mathbf{A_p}\mathbf{A_s^*},
\end{aligned} \tag{1}$$

where $\sigma_j(x) = 2\pi d_{eff}\mathrm{v_j}/\lambda_j n_j$ are the nonlinear coupling coefficients in the PP elements, while $\sigma_j(x) = 0$ within the uniformly polarized gaps, γ_j and $\beta_j \equiv \mathrm{v_j}\beta_{2,j}/2$ are the damping and dispersion coefficients. The input parameters in the model are the properties of the nonlinear medium and the pump amplitude at the input face, $\mathbf{A_p}(x = 0, t)$, generating outputs of $\mathbf{A_p}(x = L, t)$, $\mathbf{A_i}(x = L, t)$ and $\mathbf{A_s}(x = 0, t)$. The nonlinear counterpropagation dynamics in the quadratic BMOPO in the presence of group-velocity dispersion, which introduces second-order time derivatives, makes use of the numerical scheme which combines the trajectories method for the treatment of the nonlinear counterpropagatig three-wave interaction with fast Fourier transformation (FFT) to account for the group-velocity dispersion effects in the spectral domain [16].

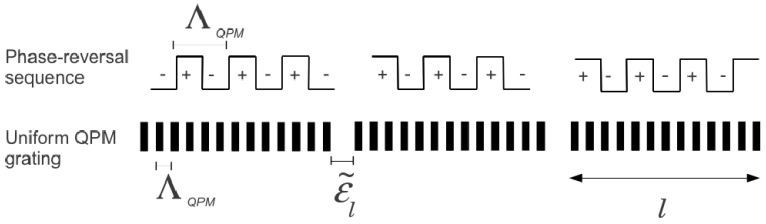

Figure 3: Quasi-phase-matching (QPM) is obtained by a phase-reversal sequence of the ferroelectric domains with a grating periodicity Λ_{QPM}. The segmented backward BMOPO is composed by a train of periodically poled GaN elements ℓ separated by uniformly polarized connection sections $\tilde{\varepsilon_\ell}$ of random lenght representing stitching errors.

The nonlinear medium is a GaN structured ensemble composed by a train of N periodically-poled GaN elements of length ℓ disposed in a straight row as shown in Fig. 3.

Simulations for this segmented structure of length $\mathrm{L_{seg}} = \mathrm{N}\ell + (\mathrm{N}-1)\tilde{\varepsilon_\ell}$, where $\tilde{\varepsilon_\ell}$ is the short random length of the gaps linking the PPGaN bricks, will be compared to the case of a continuos medium of length L= Nℓ. Two segmented structures have been simulated:
I) For L = 64 ℓ = 1.25 cm, each element has a length $\ell = 195$ μm. The segmented BMOPO will have a length $\mathrm{L_{seg}} = 1.32$ cm with 63 random gaps $\tilde{\varepsilon_\ell} = \langle\tilde{\varepsilon_\ell}\rangle + \delta\varepsilon_\ell$ where $\delta\varepsilon_\ell$ is random uniformly distributed in the interval $[-\Delta\varepsilon_\ell, +\Delta\varepsilon_\ell]$ with $\langle\tilde{\varepsilon_\ell}\rangle = 10.8$ μm for the mean value and $\Delta\varepsilon_\ell/\langle\tilde{\varepsilon_\ell}\rangle = 0.15$.
II) For L = 48 ℓ = 1.25 cm, each element has a length $\ell = 260$ μm. The segmented BMOPO will have a length $\mathrm{L_{seg}} = 1.30$ cm with 47 random gaps $\tilde{\varepsilon_\ell} = \langle\tilde{\varepsilon_\ell}\rangle + \delta\varepsilon_\ell$ where $\delta\varepsilon_\ell$ is random uniformly distributed in the interval $[-\Delta\varepsilon_\ell, +\Delta\varepsilon_\ell]$ with $\langle\tilde{\varepsilon_\ell}\rangle = 10.8$ μm for the mean value and $\Delta\varepsilon_\ell/\langle\tilde{\varepsilon_\ell}\rangle = 0.15$.
For both cases, the waveguide has a section $\mathrm{S_{eff}} = 3.6$ $\mu\mathrm{m}^2$.

We choose the three QPM waves marked on the Fig. 2, and we model BMOPO operation with a broadband stochastic pump pulse with a FWHM temporal length of 150 ps, and where the spectral FWHM width $\Delta\nu_p(0)$ centered at $\lambda_\mathrm{p} = 1.06\mu$m

varies in a large spectral bandwidth range [1.79 THz - 4.7 THz], with $n_p = 2.30856$, $v_p/c = 0.41337$, $\beta_{2,p} = 0.286$ ps^2/m; and with $\lambda_s = 1.56242\mu$m, $n_s = 2.26580$, $v_s/c = 0.41872$, $\beta_{2,s} = 0.0647$ ps^2/m; $\lambda_i = 3.29791\mu$m, $n_i = 2.12353$, $v_i/c = 0.41337$, $\beta_{2,i} = -0.418$ ps^2/m. The QPM period as low as $\Lambda_G = 335$ nm may be realized in GaN by epitaxy [12].

The pump pulse is issued from a Gaussian stochastic process translationally invariant with zero mean $\langle \mathbf{A_p}(\mathbf{x} = \mathbf{0}, \mathbf{t}) \rangle$ and exponential autocorrelation function $\left\langle \mathbf{A_p}(x = 0, t' + t)\mathbf{A_p^*}(x = 0, t) \right\rangle = \left|\mathbf{A_p^0}\right|^2 \exp\left(-|t|/\tau_c\right)$, where $\tau_c = 1/\pi\Delta\nu_p$ is the correlation time. Note that, while the pump phase fluctuations are absorbed by the idler wave thanks to the phase-locking mechanism, the generation of the signal still remains affected by the intensity fluctuations of the pump. In the presence of small group velocity difference between the pump and the signal, which is the case for the forward OPOs corresponding to Fig. 1(a), pump intensity fluctuations are partly transferred to the signal component [7, 9]. Conversely, in the presence of the strong group velocity difference of the backward OPO, corresponding to configurations of Fig. 1(b)(c), intensity fluctuations of the pump are averaged by the strong convection effect, which thus leads to an enhancement of the coherence of the backward wave [4]. The higher the incoherence of the pump, the larger the amount of coherence transfer as studied in section V.B of Ref.[6].

Stochastic BMOPO operation in both continuous and segmented structures are simulated with a pump pulse of $I_p = 2$ GW/cm^2 intensity, the BMOPO threshold intensity being $I_{p,th} = 0.937$ GW/cm^2. The peak power yields 72 W, a pulsed energy of 10.8 nJ, and a fluence of 0.3 J/cm^2 which remains below the damage threshold for GaN [18, 19]. The pump and the parametric spectra for the 64 times segmented BMOPO are illustrated in Fig 4, Fig 5 and Fig 6, for three different starting pump bandwidths.

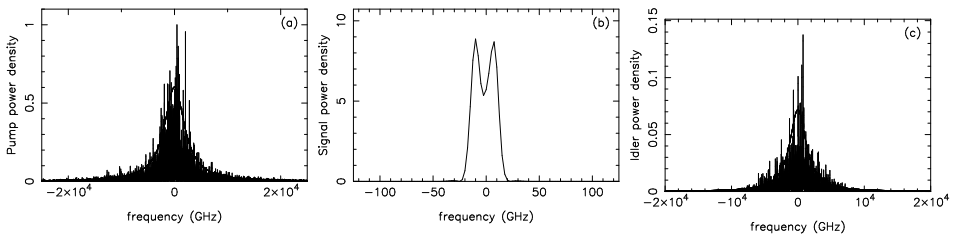

Figure 4: BMOPO (segmented in 64 elements) for a stochastic pump input of FWHM $\Delta\nu_p(0) = 3.64$ THz : (a) Output incoherent pump spectrum fitted by a Gaussian envelope of FWHM $\Delta\nu_p(\mathrm{L}) = 5.06$ THz, (b) backward signal spectrum with $\Delta\nu_s(0) = 26.75$ GHz, and (c) forward idler spectrum with a Gaussian fitting of FWHM $\Delta\nu_i(\mathrm{L}) = 3.06$ THz. The coherence gain attains $\Delta\nu_p/\Delta\nu_s = 189$ for a pump depletion or efficiency of 0.1945.

As we can see, the higher the incoherence of the pump (larger spectral bandwidth), the larger the amount of coherence transfer to the signal wave. The pump depletion or parametric downconversion efficiency versus initial pump bandwidth for the periodically polarized continuous waveguide and for both fragmented BMOPOs are shown in Fig 7, Fig 8, Fig 9, and Fig 10.

We can see that these efficiencies are of the same order for the three BMOPOs and tender to decrease when the initial pump bandwidth increases. The more interesting domain is detailed (with high discretization) in Fig 7 in the broad

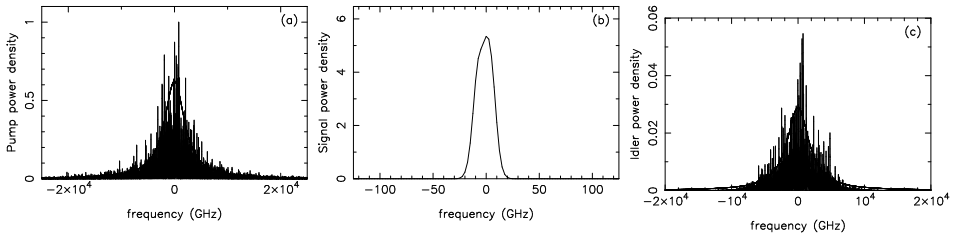

Figure 5: BMOPO (segmented in 64 elements) for a stochastic pump input of FWHM $\Delta\nu_p(0) = 4.20$ THz : (a) Output incoherent pump spectrum fitted by a Gaussian envelope of FWHM $\Delta\nu_p(\mathrm{L}) = 5.35$ THz, (b) backward signal spectrum with $\Delta\nu_s(0) = 20.25$ GHz, and (c) forward idler spectrum with a Gaussian fitting of FWHM $\Delta\nu_i(\mathrm{L}) = 4.08$ THz. The coherence gain attains $\Delta\nu_p/\Delta\nu_s = 264$, for a pump depletion or efficiency of 0.1133.

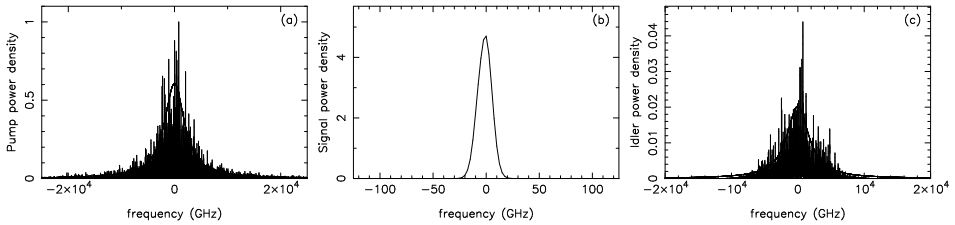

Figure 6: BMOPO (segmented in 64 elements) for a stochastic pump input of FWHM $\Delta\nu_p(0) = 4.28$ THz : (a) Output incoherent pump spectrum fitted by a Gaussian envelope of FWHM $\Delta\nu_p(\mathrm{L}) = 5.35$ THz, (b) backward signal spectrum with $\Delta\nu_s(0) = 15.87$ GHz, and (c) forward idler spectrum with a Gaussian fitting of FWHM $\Delta\nu_i(\mathrm{L}) = 4.06$ THz. The coherence gain attains $\Delta\nu_p/\Delta\nu_s = 337$ for a pump depletion or efficiency of 0.0843.

bandwidth region and low pump depletion. This small depletion avoids partial upconversion in the reversible parametric process, which would give rise to a multipeak signal [as e.g. shown on Fig 4(b)] and lower coherence transfer. Each point of Fig 7, Fig 8, Fig 9 and Fig 10, requires 7 hours CPU numerical calculation due to the combined Runge-Kutta-FFT procedure which was not necessary for the deterministic pump broadening of Ref.[4].

This is the reason for taking a rougher discretization in Fig 8, Fig 9, and Fig 10, the frequency interval between two points corresponding to 0.05 THz to 0.1 THz. This rough discretization gives rise to the serrated curves, which are more evident in the narrower input bandwidth region. The fluctuations in the efficiency comes from the complex shape of the stochastic input spectrum, composed of several high amplitude peaks. It becomes difficult to associate a single input bandwidth parameter by fitting a smooth Gaussian profile. This difficulty was avoided for the deterministic pump broadening through pump chirping of Ref.[4], as we can remark in the more smoothed curve of Fig.5. Nonintuitively, the stitched BMOPO is as efficient as the uniform quasi phase matched guided BMOPO. Its efficiency turns to be about that of the one piece periodically polarized PPGaN BMOPO, because the generated coherent phase of the backscattered wave locks the phases of the forward propagating waves in such a way that the dynamics is almost insensitive to the short uniformly polarized connection sections. The phase-locking behaviour inside the PPGaN bricks is illustrated in Fig 11.

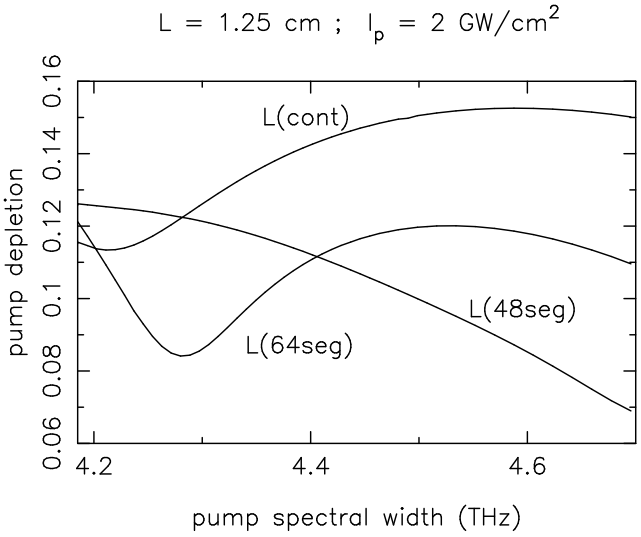

Figure 7: Pump depletion $1 - I_p(L)/I_p(0)$ versus input pump spectral width, for both segmented BMOPOs (48 segments and 64 segments) and for the one piece periodically polarized PPGaN BMOPO.

By integrating the spectra, it is found that the conversion into parametric waves for the three cases are :
1) for the input pump bandwith $\Delta\nu_p(0) = 3.65$ THz of Fig 4, $I_s(0)/I_p(0) = 0.1362 \pm 0.0004$ for the signal and $I_i(L)/I_p(0) = 0.0679 \pm 0.0002$ for the idler, while the pump depletion yields $1 - I_p(L)/I_p(0) = 0.1945 \pm 0.0006$;
2) for the input pump bandwith $\Delta\nu_p(0) = 4.20$ THz of Fig 5, $I_s(0)/I_p(0) = 0.0793 \pm 0.0004$ for the signal and $I_i(L)/I_p(0) = 0.0395 \pm 0.0002$ for the idler, while the pump depletion yields $1 - I_p(L)/I_p(0) = 0.1133 \pm 0.0006$;
3) for the input pump bandwith $\Delta\nu_p(0) = 4.28$ THz of Fig 6, $I_s(0)/I_p(0) = 0.0590 \pm 0.0004$ for the signal and $I_i(L)/I_p(0) = 0.0294 \pm 0.0002$ for the idler, while the pump depletion yields $1 - I_p(L)/I_p(0) = 0.0843 \pm 0.0006$.

To avoid other nonlinearities, such as stimulated Raman scattering, which is the most harmful nonlinearity competing with the parametric downconversion [2], we can further decrease the pump intensity. With $I_p = 1.5$ GW/cm^2 and a fluence of 0.225 J/cm^2, we obtain 15% pump depletion and a coherence gain $\Delta\nu_p(L)/\Delta\nu_s(0) = 173$.

As expected from the convection-induced phase-locking mechanism, even for the segmented stochastic BMOPO, the stochastic phase modulation in the pump is essentially transferred to the forward idler, while the phase of the backward signal is almost constant. This is further illustrated in Fig. 11 where the phase distributions of the waves are plotted inside the interaction medium for the maximum nonlinear interaction at time $t = 254$ ps. The stochastic idler phase approximately follows the phase of the pump, whereas the signal phase is almost invariant throughout the BMOPO sample.

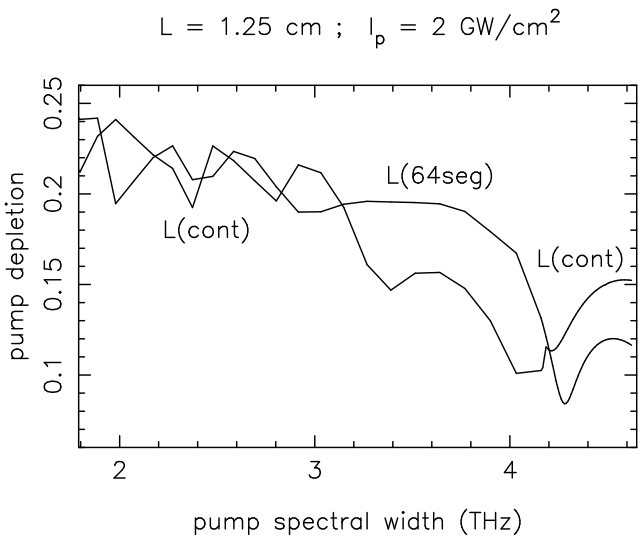

Figure 8: Pump depletion $1 - I_p(L)/I_p(0)$ versus input pump spectral width, for the segmented BMOPO of 64 segments L(64seg) compared to the one piece periodically polarized PPGaN BMOPO L(cont).

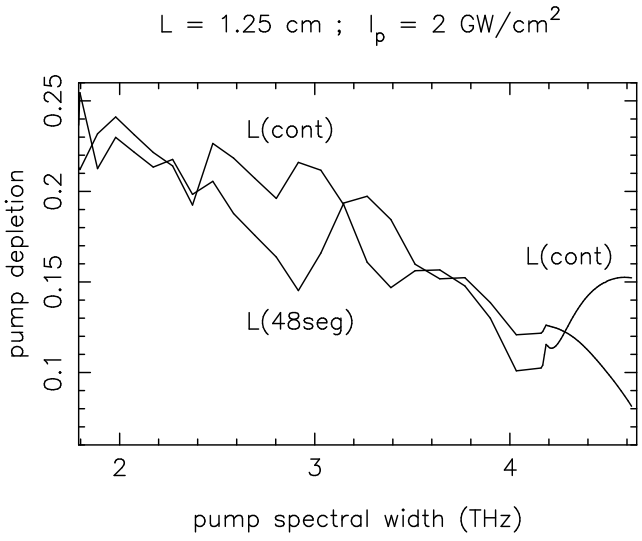

Figure 9: Pump depletion $1 - I_p(L)/I_p(0)$ versus input pump spectral width, for the segmented BMOPO of 48 segments L(48seg) compared to the one piece periodically polarized PPGaN BMOPO L(cont).

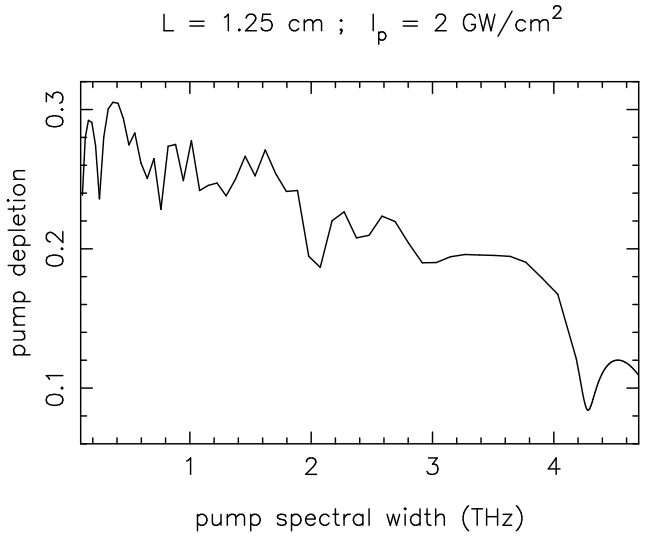

Figure 10: Pump depletion $1 - I_p(L)/I_p(0)$ versus input pump spectral width for the BMOPO of 64 segments in a large spectral bandwidth range [0.1 THz - 4.7 THz].

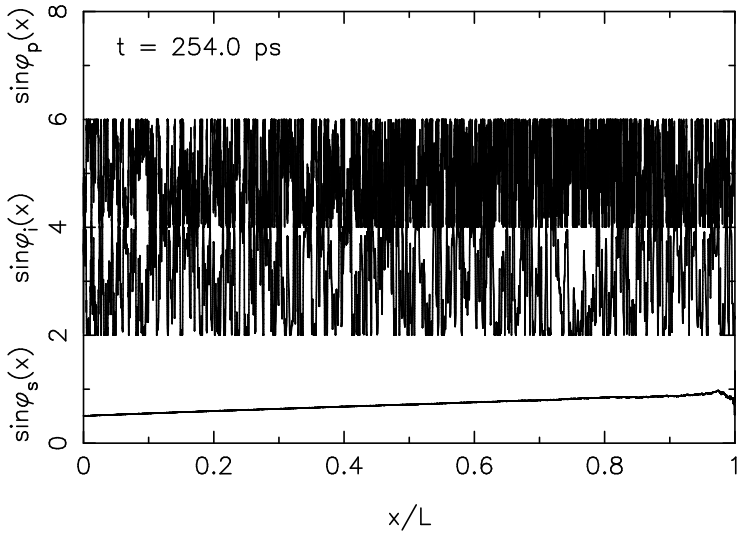

Figure 11: Phase distributions inside the stochastic segmented GaN BMOPO for the pump, the forward idler (locked to the pump), and the backward signal (almost constant), at the maximum of the interaction (at time $t = 254$ ps).

3 Summary

We have numerically simulated the dynamics in fragmented BMOPOs and realistic PPGaN waveguides by using stochastic pump pulses from 0.1 THz to 4.7 THz input bandwidth. It has been shown that mirrorless optical parametric oscillation occurs with reasonable pump power and that the coherence transfer $\Delta\nu_p(L)/\Delta\nu_s(0)$ may attain more than 330 in a 1.25 cm length waveguide. Parametric three-wave interaction is a reversible process and downconversion in one PP element could be destroyed in the adjacent one if the phase shift produced in the gap reverses the downconversion, as is the case for a standard forward OPO. Quite surprisingly in the backward BMOPO, the structure presenting stitching errors is almost as efficient as a perfect one, like that presented in [4], because the coherent phase of the backward wave locks the phases in such a way that the dynamics is almost insensitive to the random length of the uniformly polarized junctions.

References

[1] Y.I. Ding, J.B. Khurgin, "Backward optical parametric oscillators and amplifiers", IEEE J. Quantum Electron. **32**, 1574-1562 (1996).

[2] C. Canalias, V. Pasiskevicius, "Mirrorless optical parametric oscillator", Nature Photon. **1**, 459-462 (2007).

[3] G. Strömqvist, V. Pasiskevicius, C. Canalias and C. Montes, "Coherent phase-modulation transfer in counterpropagating parametric down-conversion", Phys. Rev. A **84**, 023825 (2011).

[4] G. Strömqvist, V. Pasiskevicius, C. Canalias, P. Aschieri, A. Picozzi, and C. Montes, "Temporal coherence in mirrorless optical parametric oscillators", J. Opt. Soc. Am. B **29**, 1194-1202 (2012).

[5] A. Picozzi and M. Hælterman, "Parametric Three-Wave Soliton Generated from Incoherent Light", Phys. Rev. Lett. **86**, 2010 (2001).

[6] A. Picozzi, C. Montes, M. Hælterman, "Coherence properties of the parametric three-wave interaction driven from an incoherent Phys. Rev. E **66**, 056605-1-14 (2002).

[7] C. Montes, A. Picozzi, K. Gallo, "Ultra-coherent output from an incoherent cw-pumped singly resonant optical parametric oscillator", Opt. Commun. **237**, 437-449 (2004).

[8] A. Picozzi and P. Aschieri, "Influence of dispersion on the resonant interaction between three incoherent waves", Phys. Rev. E **72**, 046606-1-12 (2005).

[9] C. Montes, W. Grundkötter, H. Suche, and W. Sohler, "Coherent signal from incoherently cw-pumped singly resonant Ti:LiNbO3 integrated optical parametric oscillators", J. Opt. Soc. Am. B **24**, 2796-2806 (2007).

[10] A. Chowdhury, H. M. Ng, M. Bhardwaj, and N. G.Weimann, "Second-harmonic generation in periodically poled GaN", Appl. Phys. Lett. **83**, 1077-1079 (2003)

[11] S. Pezzagna, P. Vennéguès, N. Grandjean, A. D. Wieck, and J. Massies, "Submicron periodic poling and chemical patterning of GaN", Appl. Phys. Lett. **87**, 062106 (2005).

[12] S. Pezzagna, J. Brault, M. Leroux, J. Massies, and M. de Micheli, "Refractive indices and elasto-optic coefficients of GaN studied by optical waveguiding", J. Appl. Phys. **103**, 123112-1-7 (2008).

[13] C. Montes, P. Aschieri, and M. de Micheli, "Backward optical parametric efficiency in quasi-phase-matched GaN waveguide presenting stitching faults", Opt. Lett. **38**, No12, 2083-2085 (2013).

[14] C. Montes, A. Mikhailov, A. Picozzi and F. Ginovart, "Dissipative three-wave structures in stimulated backscattering. I. A subluminous solitary attractor", Phys. Rev. E **55**, 1086-1091 (1997).

[15] C. Montes, A. Picozzi and D. Bahloul, "Dissipative three-wave structures in stimulated backscattering. II. Superluminous and subluminous solitons", Phys. Rev. E **55**, 1092-1106 (1997).

[16] C. Montes, P. Aschieri, and A. Picozzi, "Model for Coherence Transfer in a Backward Optical Parametric Oscillator", SPIE Proc. **8011**, 801136-1-10 (2011).

[17] M. Monerie, "Propagation in doubly clad single-mode fibers" IEEE J. Quantum Electron. **18**, 535 (1982).

[18] X.C. Wang, G.C. Lim, F.L. Ng, W. Liu, and S.J. Chua, "Femtosecond pulsed laser-induced periodic surface structures on GaN/sapphire", Applied Surface Science **252**, 1492-1497 (2005).

[19] K. Ozono, M. Obara, A. Usui, and H. Sunakawa, "High-speed ablation etching of GaN semiconductor using femtosecond laser", Optics Commun. **189**, 103-106 (2001).